Faraday Discussions

Spiers Memorial Lecture: Water at Interfaces

Journal:	*Faraday Discussions*
Manuscript ID	FD-ART-08-2023-000147.R1
Article Type:	Paper
Date Submitted by the Author:	23-Aug-2023
Complete List of Authors:	Devlin, Shane; University of California Berkeley, Chemistry; Lawrence Berkeley National Laboratory, Chemical Sciences Division Bernal, Franky; University of California Berkeley, Chemistry; Lawrence Berkeley National Laboratory, Chemical Sciences Division Riffe, Erika; University of California Berkeley, Chemistry; Lawrence Berkeley National Laboratory, Chemical Sciences Division Wilson, Kevin; Lawrence Berkeley National Laboratory, Chemical Sciences Saykally, Richard; University of California Berkeley, Chemistry; Lawrence Berkeley National Laboratory, Chemical Sciences Division

SCHOLARONE™
Manuscripts

THE SPIERS MEMORIAL LECTURE: WATER AT INTERFACES

Shane W. Devlin[1,2], Franky Bernal[1,2], Erika J. Riffe[1,2], Kevin R. Wilson[2], Richard J. Saykally[1,2]

1: Department of Chemistry, University of California, Berkeley, CA 94720, USA.

2: Chemical Sciences Division, Lawrence Berkeley National Lab, Berkeley, CA 94720, USA.

Introduction

The aqueous interface is a central element in ubiquitous modern contexts involving chemical and physical processes, as well as biological systems and physiology.[1–5] A deeper understanding of the interfacial behavior of water is therefore imperative for characterizing phenomena as diverse as water freezing and evaporation, desalination, gas solubility, thundercloud charging, droplet chemistry, protein folding, the structure and function of biological membranes and membrane proteins, Hofmeister effects, aqueous electrochemistry, and on-water organic catalysis. In this article, we discuss some of the current issues and recent advances addressing these subjects. In the interest of brevity, we refer to recent papers on these subjects, implying that readers should consult the references cited therein for additional details.

We begin by briefly describing recent advances in techniques employed for experimental characterization of aqueous interfaces. Principal among these is second-order nonlinear laser spectroscopy, encompassing second harmonic generation (SHG) and sum frequency generation(SFG), as these are highly surface specific. Nevertheless, exciting advances have also been made in the development and application of X-ray spectroscopy and scanning probe techniques, as well as new approaches to sample introduction and manipulation.

Vibrational Sum Frequency Generation Spectroscopy

Characterizing the three-dimensional spatial distribution of molecules at aqueous interfaces is central to understanding processes ranging from membrane biophysics to atmospheric chemistry. While several techniques can reveal surface composition, obtaining information on the depth distribution is particularly challenging. For example, X-ray photoelectron spectroscopy can achieve both element-selective and depth-resolved profiling of interfaces by varying the kinetic energy of the outgoing photoelectrons, but the method nevertheless is limited to quite large probe depths (ca. 10 nm).

Vibrational sum frequency spectroscopy(VSFGS) has become a powerful and popular technique for probing the chemical vibrations of molecules present at the outermost layers of interfaces, providing orientation information and quantitative depth resolution.[6] For example, Yu et al. recently demonstrated the technique on formic acid molecules residing at the air-water interface.[7] With increasing mole fraction from 2.5% to 10%, the formic acid molecules shift, on average, ∼0.9 Å deeper into the bulk. The agreement with simulation results indicates that modern heterodyne-detection versions of VSFGS achieve depth resolution at the Ångstrom-scale.

Deep UV-Electronic Sum Frequency Generation Spectroscopy

As a general means of directly detecting and characterizing the adsorption of ions to aqueous interfaces, the Saykally group has extended the well-known surface-selective techniques of second harmonic generation[8] and sum frequency generation[9] spectroscopies into the deep-ultraviolet. This permits exploitation of the strongly allowed electronic transitions in atoms and molecules to be exploited for resonant enhancement and thus for selective excitation in aqueous media. For example, charge transfer to solvent (CTTS) transitions in anions like iodide and

thiocyanate can be monitored as a function of bulk concentration to yield Gibbs free energies of adsorption and solvent shifts, which can be directly compared with theoretical calculations to characterize these ion adsorption phenomena, which both theory and VSFG studies previously claimed to be impossible.

Soft X-Ray Second Harmonic Generation as an Interfacial Probe

While X-ray photoelectron spectroscopy has been exploited as a near-surface probe of interfaces for many years, interpretation of results from these experiments has often been problematic due to the large probing depths. With the goal of combining the atom-selective nature of X-ray core-level transitions and the extreme surface selectivity of second harmonic generation, Lam et al.[10] utilized the Trieste free electron laser facility for the first demonstration of soft X-ray SHG. In that work, the graphite/air interface was studied, providing a detailed characterization of this new highly surface-selective probing method, anticipating application to aqueous interfaces in subsequent experiments.

Scanning Probe Microscopy

Using their novel design of an ultrahigh resolution atomic force microscopy (AFM) system operated in frequency modulation mode, Schlesinger and Sievan[11] significantly extended measurements of the force acting between hydrophobic surfaces immersed in water to shorter distances-all the way to contact, revealing qualitatively new behavior as the two hydrophobic surfaces begin to attract each other each other in the aqueous medium. The system was designed specifically for the study of hydration layers and ion organization next to solid surfaces and biomolecules. Subsequent studies provided the first detailed 3D maps of the solvation/hydration layer of two archetypal hydrophobic surfaces: graphite (HOPG) and self-assembled fluoro-alkane monolayer (FDTS). In degassed solutions, they find different tip–surface interactions for the two surfaces; hydration oscillations superimposed on van der Waals attraction with HOPG and electrostatic repulsion with FDTS. Both are similar to interactions observed with hydrophilic surfaces.

Nonlinear Light Scattering Spectroscopy

The large surface-to-volume ratio of micro- or nanoparticles and droplets greatly alters their interfacial properties compared to those of bulk or planar counterparts. These properties are therefore not fully exploited by traditional surface-sensitive nonlinear spectroscopies, e.g. SFG or SHG, which probe materials in reflection or transmission geometries. Rather, the scattering versions of these techniques, viz. vibrational sum frequency scattering spectroscopy (VSFSS) and femtosecond second harmonic scattering (fs-SHS) can probe the interfacial properties of collections of micro- or nanoparticles and droplets *in situ*.

Within the last decade, second harmonic scattering (SHS) methods have moved beyond simply probing the buried interfaces of colloidal microparticles and droplets. The development of SHS techniques, including polarization- and angle-resolved SHS (AR-SHS), have engendered a new understanding about adsorption kinetics[12], electrostatic and surface properties[13], structure of the

electric double layer (EDL)[14], and the orientation of water molecules at the interface[15]. Furthermore, Gomopoulos et al. designed an improved optical scheme exploiting the fact that SH efficiency scales quadratically with pulse energy. The signal-to-noise improvement made it possible to effectively study biologically relevant systems with label-free or non-resonant SHS.[16]

Similarly, VSFSS has emerged as a useful method for a variety of applications since its first observation from particles in liquid by Roke et al. in 2003.[17] More recently, VSFSS has been used to determine the mechanism for the stability of "uncharged" nanoemulsions[18] as well as how layer-by-layer deposition of polyelectrolytes can be understood to make nanoemulsions with tunable stability and interfacial properties[19]. Using isotopic dilution in combination with VSFSS, Pullanchery et al. found that water has a stronger hydrogen-bonding network near the oil-nanodroplet interface, whereas traditional VSFG in reflection geometry has produced conflicting results[20]. However, more work needs to be done to study aerosol particles with VSFSS, as the detection limits of such experiments have been recently debated.[21]

1. DYNAMICS AND NANO-RHEOLOGY OF INTERFACIAL WATER

While we have made progress in understanding the static properties of interfacial water, water is in motion for many naturally occurring phenomena (raindrops falling, rivers flowing, etc.) and technological applications (water traversing membranes in water purification, desalination). At the nanoscale, the description of water in terms of its macroscopic properties (density, viscosity, etc.) breaks down, and novel concepts and experimental approaches are needed to further our understanding.

A. THE STRUCTURE OF INTERFACIAL WATER

The simplest aqueous interface is that formed by water in its liquid and vapor forms, which has accordingly been examined in detail both theoretically and experimentally by many groups. We begin by elaborating on the nature of this fundamental interface, focusing on the most recent results, and adopting the "instantaneous interface" concept of Willard and Chandler[22] as the reference for structural and dynamical properties, since fluctuations in the interfacial region can be large, and distort the structural and dynamical properties referenced to an "average interface", e.g. the traditional sigmoidal Gibbs dividing surface (GDS).

One of the most profound manifestations of utilizing the instantaneous interface description is the appearance of molecular *layering*, indicating that the liquid-vapor phase boundary is describable as a sharp surface with a width of ca. a molecular diameter dividing the bulk liquid and vapor phases. Here, we adopt the language and description of Kessler et al.[23] for simplicity, noting that the recent study of Odendahl and Geissler[24] refines and elaborates this description, with updated references. We also note several other influential reviews.

The layering of the room temperature interface is shown in terms of density profiles in Fig. 1. As shown in Figs. 1 and 2, and demonstrated in both theoretical[22–24] and experimental[25] studies, the topmost layer(L0) of the water surface is dominated by single hydrogen bond(HB) donor (SD) water configurations with *dangling* OH bonds preferably extending out of this layer into the vapor phase, while at the same time serving as an H-bond acceptor and donor for the adjacent layer (L1). This second water layer can be further divided into L1(2) where the

orientation of the water molecules is inverted with respect to L0, and a novel interlayer($L1^{\shortparallel}$). Specifically, in L1, one of the OH bonds is preferentially pointing toward the bulk-like L2 layer while simultaneously accepting and donating H bonds from L0 and $L1^{\shortparallel}$. In this latter water layer, the molecules are oriented parallel with respect to the water/vapor interface and are able to form H bonds with L0 and L1 as well as forming particularly strong intralayer H bonds within $L1^{\shortparallel}$. The water molecules in L2 are already structurally disordered and resemble bulk water, with a relatively weak orientational correlation that is similar to L0. All layers beyond L2 obey no structural order and therefore correspond to bulk liquid water. All of this implies that only the topmost ~5 Å of the interface exhibits structural order. Kessler et al.[23] emphasize that L0 cannot be understood as a liquid water layer, but rather as a sparse population of water molecules with a higher proximity to the vapor than to the first dense layer L1; despite their equal volumes, L0 consists only of about 10–20% of the water molecules in L1.

The layered structure of this interface engenders important capabilities for chemical and physical processes and reactions. For example, the mechanism of gas adsorption depends explicitly on the presence of accessible interfacial vacancies, and as elaborated in the Charged Interfaces section, the formation and dynamics of interfacial protons engenders “proton wires” parallel to the outermost water layer.

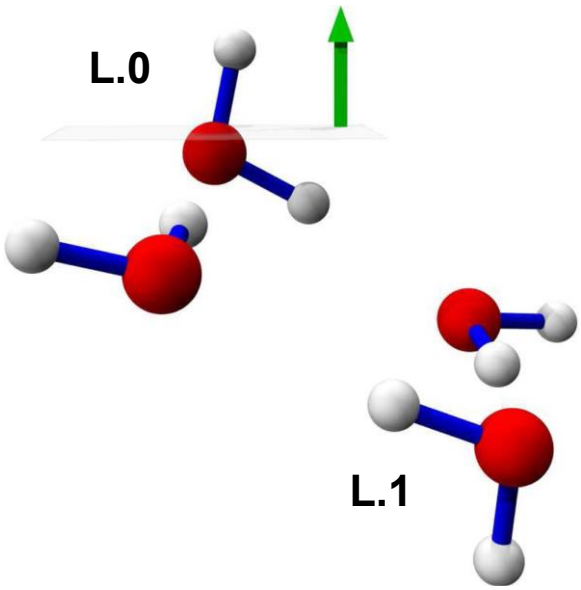

Fig 1: Structure of the room temperature liquid/vapor interface from the MD simulations of Ref. 23. The topmost water molecule represents layer L0, while the lowest constitutes layer L1. The interjacent molecules correspond to $L1^{\shortparallel}$. The green arrow designates the surface normal. See text for full details. Reproduced from reference 23 with permission from the American Chemical Society, copyright 2015.

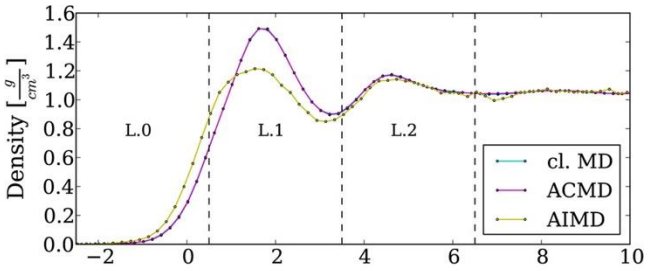

Fig. 2: Density profiles vs distance (Å) showing instantaneous water layers (L0–L2) as indicated by vertical dashed lines for cl. MD (conventional molecular dynamics), AIMD (ab initio molecular dynamics, and ACMD (quantum mechanical molecular dynamics). See text for full details. Reproduced from reference 23 with permission from the American Chemical Society, copyright 2015.

As a result of the broken hydrogen bond structure, the dynamics of interfacial water differ considerably from those in the bulk liquid.[25] The reorientational motion of free OH groups at the air/water interface was measured using time-and polarization-resolved sum frequency generation spectroscopy[25] to be ca.1 ps, 3 times faster than that occurring in the bulk, and exhibited a diffusion-like behavior, quite unlike the motions exhibited by the liquid. Accompanying simulations showed that in-plane and out-of-plane reorientational diffusion coefficients were comparable.

The role of nuclear quantum effects on the hydrogen bond dynamics, in the form of quantum tunneling and zero-point oscillations, have been addressed in considerable detail for bulk water phases, but are not yet well-understood for aqueous interfaces; Kessler et al. describes them as "minimal", save for libration. Two such interesting phenomena are the isotope fractionation that occurs between the liquid and vapor in the evaporation process, observed by Cappa et al.[26] and addressed via theoretical calculations by several groups[23], and the fact that, compared with bulk water, the average O–O distance is increased because of relaxation effects at the water/vapor interface.[27] The librational frequency of interfacial water was recently observed by vibrational sum frequency spectroscopy to increase significantly relative to its bulk value, indicating a stiffer interfacial rotational potential due to termination of the H-bond network.[28] The effects of librational excitation on hydrogen bond lifetimes have recently been studied in water clusters and shown to result from dramatic increases in the quantum tunneling splitting accompanying excitation of librational motions.[29,30]

B. EVAPORATION OF WATER

Understanding the details of water evaporation and condensation remains an unsolved problem of central importance in science. Despite decades of study, the rates and mechanisms of these processes remain incompletely understood, particularly in the case of aerosol droplets containing ions and surfactant molecules, where they govern cloud droplet growth kinetics, and in turn, aerosol formation and cloud radiation properties in our atmosphere.[31]

The kinetics of evaporation and condensation processes are governed by the evaporation (γ) and condensation (α) coefficients. Those coefficients are empirically determined ratios of the

observed molecular flux evaporating from or condensing onto the liquid surface to the theoretical maximum value permitted by gas kinetic theory. For evaporation, this is described by the Hertz-Knudsen equation:

$$J_e = \gamma \frac{p_{sat}}{\sqrt{2\pi m k_B T_{surf}}}$$

Here J_e is the evaporative flux, p_{sat} is the saturation vapor pressure of the liquid, T_{surf} is the surface temperature of the liquid, m is the molecular mass of the evaporating molecule, k_B is the Boltzmann constant, and γ is the evaporation coefficient. Because the present work only concerns the study of evaporation rates, we will eliminate the condensation coefficient and mass accommodation flux from further discussion except to note that there is an analogous Hertz-Knudsen equation for condensation. Additionally, microscopic reversibility requires the condensation and evaporation coefficients for a single system to be equal.

An evaporation coefficient of unity describes a system operating at the theoretical maximum rate of evaporation with no energetic barrier. An evaporation coefficient of less than unity then describes a system with some kinetic or thermodynamic barrier, such as proceeding through a transition state or a specific orientation that has an associated energetic barrier. As such, determining an accurate value for γ can yield valuable insight into the molecular mechanism of evaporation.

The Cohen and Saykally groups have developed an experimental technique that avoids many previously reported experimental complications, such as stagnant water surfaces and direct contact thermocouples,[32] employing a narrow liquid microjet modified to generate a constantly renewing droplet train that is injected in vacuum and studied with Raman Thermometry to provide a clean droplet surface and condensation-free evaporation conditions. Using this technique, this work has determined the evaporation coefficient of pure water(both H_2O and D_2O) to be 0.62 ± 0.09, a value which indicates a small kinetic or energetic barrier to the evaporation process.[33] This technique was also used to study the effects of several inorganic ions on the evaporation rate.[34–36] Duffey et al. studied the evaporation rate of aqueous acetic acid solutions in an attempt to investigate the effects of hydrocarbon surfactants, but found no deviation from that of neat water.[37] In fact, until the recent study of HCl solutions[31], the only aqueous solution exhibiting a statistically significant decrease from the pure water value was 4 M sodium perchlorate, which exhibited $\gamma = 0.47 \pm 0.02$ – a ~25% decrease.[35]

The recent study by Rizzuto et al.[31] addresses the effect of bulk pH on the evaporation rate of water, and accordingly provides additional insight into the controversial subject of the water surface pH, discussed in the following section on charged interfaces. The measured evaporation coefficients of HCl solutions exhibited wide variations with concentration, with 1.0 M samples yielding $\gamma = 0.24 \pm 0.04$, a 60% decrease, while a 0.1M sample yielded $\gamma = 0.91 \pm 0.08$, a 45% *increase* relative to pure water (at 95% confidence). These results suggest a significant perturbation on the interfacial structure induced by hydronium ions, or perhaps by ion pairing with chloride.

In addition to experimental studies, computational modeling has been performed by many groups.[38,39] Since evaporation is a very rare event, some studies have taken advantage of the microscopic reversibility of the system and determined a mass accommodation coefficient. The above experimental results conflict with both transition path sampling calculations[38] and some MD simulations, and even recent reinterpretations of the data[40], which conclude that there is no kinetic barrier to evaporation or condensation of pure water, such that the value of γ is necessarily unity . More recently, Nagata et al.[39] used detailed MD simulations at the water/air

interface to show that the evaporation of water does indeed engender a large energetic barrier, and is enabled by concerted, ultrafast hydrogen bond dynamics of interfacial water. They conclude that the high kinetic energy of an evaporated water molecule is enabled by well-timed making and breaking of hydrogen bonds involving at least three water molecules at the interface, the recoil of which allows one of the molecules to escape. The above illustrates how having a generally accepted evaporation coefficient has remained elusive among the scientific community for decades and motivates the need for continued research into the mechanistic details of water evaporation and condensation.

2. ELECTRIFIED/CHARGED AQUEOUS INTERFACES

Interfaces are often charged, because of the intrinsic charge of the material interface and membrane interface, as well as the emergence of the counter charge as a response of the water pH. In electrochemistry, charge is applied to drive molecular orientation, charge transfer, and chemical transformation. These interfaces induce ion condensation, generating the electrical double layer – Stern layer and diffuse layer Although it is evident that the molecular organization at electrochemical and electrified interfaces determines the chemistry occurring at these interfaces, the description of these processes still occurs at a mean-field level. Is that sufficient?

Gonella et al.[41] have published a recent and comprehensive review on the behavior and current status of our understanding of water at charged interfaces. Many open questions remain regarding the molecular picture of the interfacial organization and preferential alignment of water molecules, as well as the structure of water molecules and ion distributions at different charged interfaces, ranging from living tissues and catalytic membranes to metals. This diversity in substrates has led to different communities considering each of these types of aqueous interface. By considering water in contact with metals, oxides and biomembranes, Gonella et al. emphasize the similarities of these systems. While in each case, classical mean-field theories can explain many macroscopic and mesoscopic observations, such theories fail to explain phenomena for which details of molecular properties are crucial. The current knowledge and limitations in our understanding as well as future opportunities are presented.

Here we describe some additional important phenomena relevant to this discussion.

A. pH AND ELECTRIC CHARGE OF THE AIR/WATER INTERFACE

Many vital chemical and physical phenomena are profoundly affected by both the charge and the intrinsic acidity/basicity of the free liquid water surface (air/water interface), yet it remains an active and controversial subject. Macroscopic bubble and droplet experiments have been interpreted to indicate a negatively charged air/water interface covered with hydroxide, whereas most recent molecular-scale studies produce the opposite conclusion, viz. that hydroxide is repelled from the interface while hydronium is strongly adsorbed. We reported results from resonant UV second harmonic generation (SHG) experiments[42] that are best modeled by surface depletion of hydroxide and establish at most a weak surface adsorption. This finding is consistent with our earlier SHG measurements indicating surface enhancement of hydrated protons[43], as well as with most[44–47], but not all[48], molecular-scale experiments, and most[49], but not all[50] recent simulations. The detailed nature of interfacial protons was elaborated by elegant sum frequency

generation experiments and theory[46], revealing that both the Zundel and Eigenn forms coexist at the interface.

Theoretical elaboration of the nature of interfacial protons and hydroxide ions was developed in terms of the instantaneous interface[51,52], described in Section I. The results of the most recent simulation[52] revealed that the layered structure of the instantaneous interface accommodates protons in the topmost later, forming extended chains, but in contrast to the previously reported single ion enrichment, it was shown that *both* protons and hydroxide prefer to accumulate in the interface at different interfacial depths - producing a double-layer ionic distribution within ~1 nm below the Gibbs dividing surface. Hydronium ions are preferentially adsorbed in the topmost layer of the interface, but hydroxide is enriched in the deeper interfacial layers, and at a higher equilibrium concentration due to its more negative free energy of interfacial stabilization (–0.90 (OH^-) vs. –0.56 (H_3O^+) kcal/mol). The air/water interface is therefore negatively charged, in agreement with macroscopic experimental observations. This work thus presents an elegant and self-consistent explanation for the long-standing controversy about the electric charge and acid-base nature of the air-water interface.

B. ION ADSORPTION TO AQUEOUS INTERFACES

Until the advent of advanced molecular dynamics simulations, the conventional view of ion adsorption to water-hydrophobe interfaces, including the air/water interface, was embodied in Onsager-Samaras theory, viz. that all ions would be repelled from such interfaces due to the construction of “image charge repulsion” forces. This would imply, for example, that the ocean surfaces would be devoid of ions, imposing a serious constraint on atmospheric and sea-spray aerosol chemistry. The picture began to change dramatically when Jungwirth and Tobias published their highly controversial results[53], proposing that highly polarizable ions, such as iodide, would *preferentially* reside at the air/water interface, while “hard”, non-polarizable ions would be repelled in the classic sense. This prediction was met with considerable resistance from the physical chemistry community, and several experiments were interpreted as disproving it.[54]

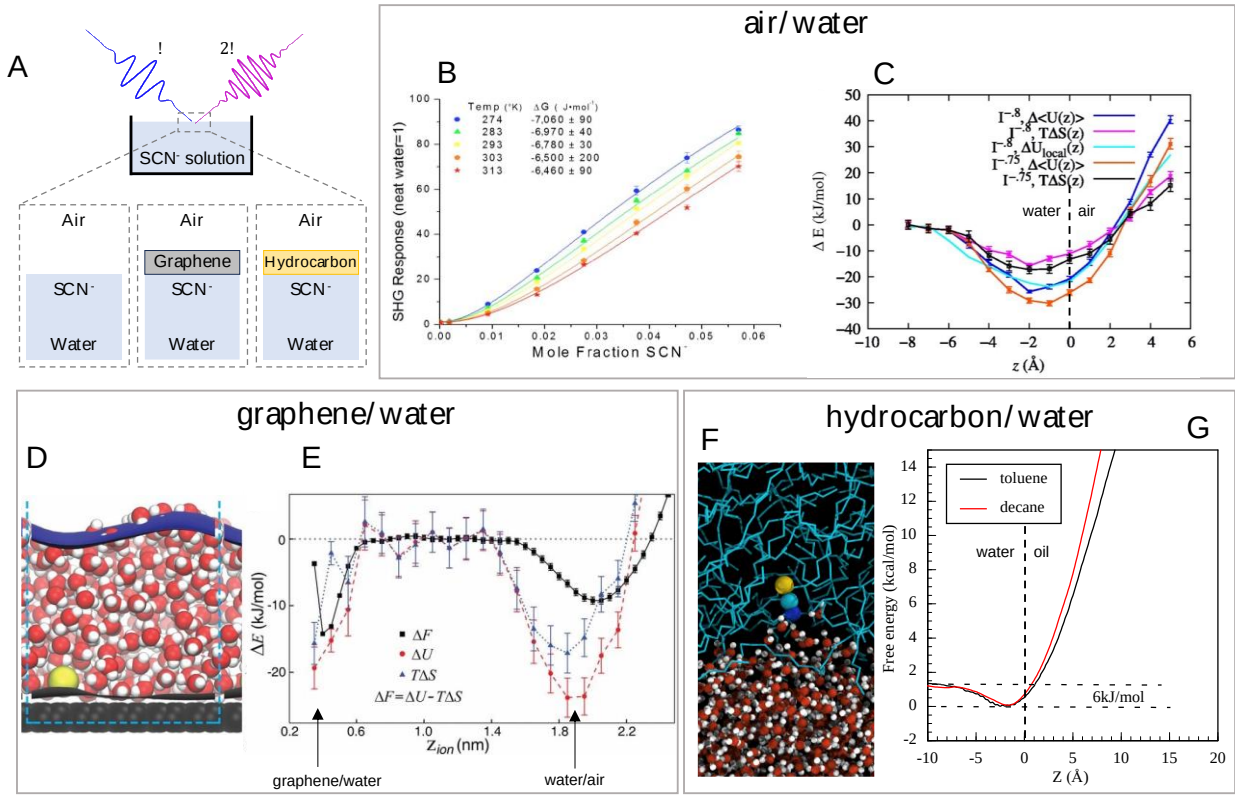

Fig 3: Ion adsorption mechanism to aqueous interfaces. **(A)** schematic of SHG experiments for air/water, graphene/water, and hydrocarbon/water studies. **(B)** Temperature-dependent SH intensities for SCN^- adsorption to the air-water interface. Ion free energy plotted against ion height in the simulation slab (GDS = 0) for **(C)** air/water, **(E)** graphene/water, and **(G)** hydrocarbon/water interfaces from MD simulation. Representative snapshots for anion adsorption to the **(D)** graphene/water and **(F)** decane/water interface. Please refer to the respective publications for full figure details. Reproduced from references 56, 58, 60 with permission from the National Academy of Sciences, copyright 2012, 2017, 2022.

Peterson et al.[8,55] designed a highly surface-selective SHG experiment that directly probed the CTTS transition of ions, and unambiguously determined that some ions do, in fact, preferentially adsorb to the air/water interface. Otten et al.[56] subsequently established the mechanism by which specific ions prefer to reside at the interface, demonstrating that a negative enthalpy drives weakly hydrated ions to the interface, shedding one or more waters of hydration in the process, which form stronger water-water bonds as part of the bulk water-network, than they were held by the ion charge (termed "solvent repartitioning"); this favorable enthalpy change is countered by an unfavorable(positive) entropy, involving the suppression of capillary waves by the ion moving to the surface (Fig 3B and 3C). Details of this proposed mechanism are still under some debate[57], but it is generally regarded as being essentially correct, augmenting the mechanism proposed by Jungwirth and Tobias[53], primarily by replacing *high polarizability* with *weak hydration* as the principal criterion for ion surface activity.

This approach to address the mechanism for ion adsorption to the air/water interface was extended to hydrophobic material surfaces by McCaffery et al.[58], wherein the adsorption of the prototypical chaotrope, thiocyanate, to the water/graphene interface was examined by deep UV

SHG measurements, which determined a Gibbs free energy of adsorption within error of that determined for air/water. Unlike for the air/water interface, wherein repartitioning of the solvent energy drives ion adsorption, computer simulations revealed that direct ion/graphene interactions dominate the favorable enthalpy change (Fig 3D and 3E). Moreover, the presence of graphene sheets themselves dampens the capillary waves, such that rotational anisotropy of the solute, if present, becomes the dominant (unfavorable) entropy contribution.

These ion adsorption studies were extended to oil/water interfaces by Devlin et al.[59,60], wherein the mechanism for SCN^- adsorption to the prototypical water/toluene and water/decane interfaces was examined by DUV-SHG spectroscopy and computer simulations, and compared with the results for SCN^- adsorption to the air/water interface. For these systems, no relative spectral shift in the charge transfer to solvent spectrum of SCN^- was observed, and the Gibbs free energies of adsorption for these different interfaces all agreed within error. Molecular dynamics simulations were applied to develop a molecular-level understanding of the adsorption mechanism and showed that the adsorption for SCN^- to both water/toluene and water/decane interfaces is driven by an *increase in entropy*, with very little enthalpic contribution (Fig 3F and 3E). This is a qualitatively different mechanism than reported for thiocyanate adsorption to the air/water and graphene/water interfaces, wherein a favorable enthalpy change was the main driving force, against an unfavorable entropy change.

These ion adsorption studies were also extended to different aqueous interfaces[61] and different surface active ions[62].

C. STRUCTURE OF METAL/WATER INTERFACES

The structure and organization of water and ions at metal/water interfaces has been the focus of many theoretical and experimental studies. From the viewpoint of fundamental physics, it is compelling to study the interaction of the strong water dipole with a charged surface, to understand how electric fields and molecular structure influence the resulting hydrogen bonding network and chemical reactivity. Specifically, it has been noted that the water-metal interaction energy is of similar magnitude to the water-water interaction energy, and that the resulting structure at the metal-water interface is determined by a fine balance of these competing forces, and by the structure of the metal itself.

Computational methods have led to significant insight into this topic, including work from the Chandler group, who first applied the methodology of the instantaneous interface to describe reorganization dynamics and density fluctuations of waters adjacent to the metal surface.[63–65] The interplay between water/metal and water/water energetics is highlighted in Fig. 4, which displays snapshots of the Pt 100 (4-fold coordinated) and Pt 111(6-fold coordinated) crystal faces, and the resulting adjacent water structure. Panels 4B and 4D illustrate the influence that the structural motifs of water directly adjacent to the metal surface have on properties such as wetting. For other comprehensive reviews on the topic, the reader is referred to references 66–68.

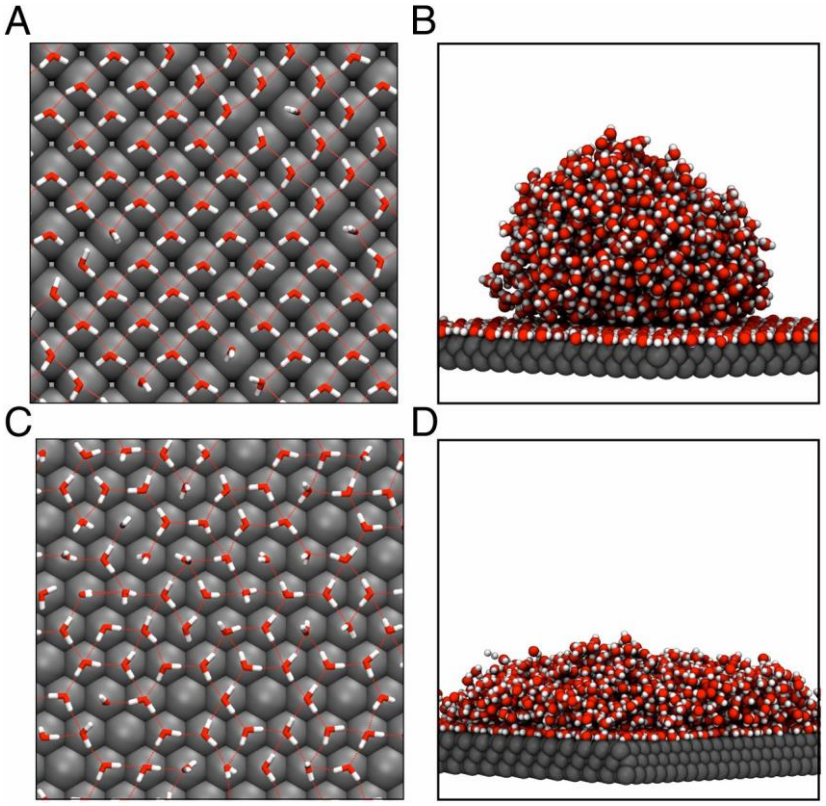

Fig 4: Comparison of the Pt(100) (A and B) and Pt(111) (C and D) crystal faces and adjacent water structure from MD simulations. Reproduced from reference 63 with permission from the National Academy of Sciences, copyright 2013.

The structure and organization at metal/water interfaces becomes more complex when one considers ionic aqueous solutions, systems with obvious applications to electrochemical energy generation and energy storage. Ion condensation at the charged metal surface forms an electrical double layer (EDL), which is partitioned into counter-ions adsorbed at the metal surface (Stern layer) and the network of mobile ions loosely bound to the interface from the surface charge (diffuse layer). The diffuse layer is a concentration-dependent entity and acts to screen electrical charge form the surface, thus reducing the local potential of the solution. Many efforts have been made to understand ion mobility, charge transfer, and adsorption of aqueous solutions to the metal/water interface, with some recent advances in experimental methods offering promising new insights. For example, Petersen and co-workers[69] have recently reported a new methodology for the application of VSFG spectroscopy to study the gold/water surface under electrochemical conditions, and unambiguously observed for the first time the OH stretch of water at a metal/water interface. Others have used VSFG to measure Stark shifts of self-assembled monolayers (SAMs) at metal/water interfaces as an indirect probe of the interfacial potential[70,71], as well as investigated other interesting systems such as the electrode/ionic-liquid interface[72]. X-ray photoemission spectroscopy has also proven to be a powerful tool for studying EDL formation at electrochemical interfaces, but for brevity we refer the reader to some of those works directly.[73–76]

D. ELECTROKINETICS

Micro- and nanofluidic devices have shown promise for energy conversion and have received significant attention over the past few years. For instance, electrokinetic streaming currents can be produced by forcing water through porous materials or through well-defined micron- or nanometer-sized channels. Duffin et al.[77,78] have shown that liquid microjet electrokinetics permit the conversion of hydrostatic pressure directly into electrical energy and molecular hydrogen and also increase the conversion efficiency (>10%) by eliminating back conduction due to electroosmotic flow with the formation of droplets at the capillary exit due to Rayleigh instabilities. Electrokinetics have also been shown to provide a novel means of detecting spectra of ions in flowing solutions.[79,80]

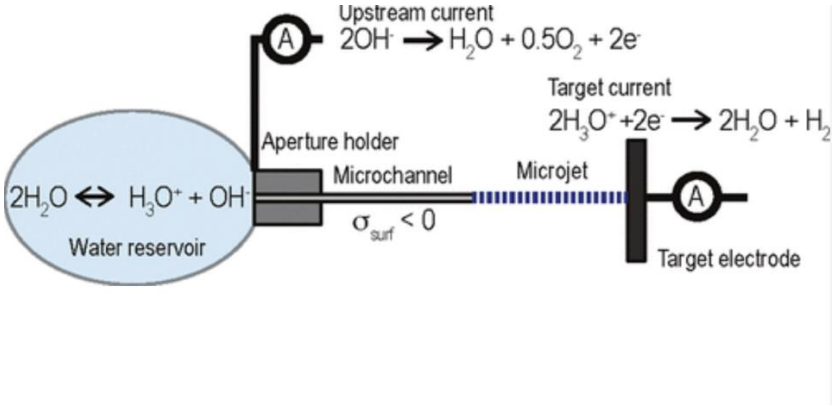

Fig 5: Experimental design of liquid microjet electrokinetics apparatus. Reproduced from reference 81 with permission from the American Chemical Society, copyright 2016.

It has long been recognized that the streaming currents arise from the asymmetric distribution of anions and cations in an interfacial electric double layer. Schwierez et al.[81] provided a highly detailed model of electrokinetic streaming currents generated from water flowing through micron-sized channels (see Figure 5), focusing on modifications of surface properties with the goal of increasing the energy conversion efficiency. The combination of a Poisson–Boltzmann description, continuum hydrodynamics, and microjet electrokinetic experiments provides detailed insight into the contribution of both electrostatic and non-electrostatic interactions to the streaming current. Specific adsorption of hydronium and hydroxide leads to anomalous ion-specific electrokinetic effects at *uncharged* surfaces, resulting in a streaming current of ~1.8 pA. However, this non-electrostatic contribution is negligible when compared to that of long-ranged electrostatic interactions at *charged* surfaces, such as those employed in[82], which result in streaming currents that are orders of magnitude larger (10–100 nA). In a negatively charged channel, the streaming current originates from the extended double layer formed from electrostatic interactions and by the preferential adsorption of hydronium to the solid/liquid interface. This more detailed model revises that suggested by Duffin et al., which proposed that hydroxide was preferentially adsorbed to the channel walls and the sole cause of the streaming current. This previous model neglected to account for the channel's intrinsic negative surface charge density. Specific ion adsorption becomes important for ions with high surface affinity ($V_S \gg k_B T$), and the interfacial affinity can be quantified using ultra-dilute salt solutions.

Tuning the surface properties of the channel, via silanization, provides a method for reversing the surface charge, thereby reversing the sign of the streaming current and switching between hydronium or hydroxide as the main charge carrier. Similarly, tuning the surface coating such that the surface charges are minimized results in a significant reduction in the streaming current, an effect that can be exploited to minimize interference by the streaming potential in liquid microjet X-ray and UV photoemission spectroscopy experiments.

Several approaches for increasing the efficiency of the electrokinetic power conversion have been explored and published, including microjet array[83], soft interfaces[84], and coated silica interfaces[81].

E. CHEMICAL REACTIONS AT AQUEOUS INTERFACES

In this section, we exploit much of the knowledge summarized in the previous sections, e.g. structure and dynamics of the water surface, mechanism of ion adsorption to aqueous interfaces, to describe perhaps the most important phenomenon engendered by the formation of these interfaces, viz. the dramatic acceleration of interfacial chemical reactions**.** Many chemical and photochemical reactions are accelerated when they occur at aqueous interfaces (including oil-water emulsions and other dispersed systems, aerosols, sprays, water droplets, and extended air-water interfaces), in comparison with corresponding reactions in gas-phase or bulk water - a phenomenon designated as "on-water" catalysis.[85] The immense potential importance of this catalytic enhancement in the fields of atmospheric chemistry, synthetic organic chemistry, as well as related research exploring the origins of life are obvious. The reasons underlying the reported rate accelerations currently remain unclear, despite considerable recent attention, but it is obvious that physicochemical concepts operating in bulk phases are not always applicable at interfaces[86], as the latter are disordered systems of nanometric thickness displaying sharp configurational fluctuations. The recent review of Ruiz-Lopez et al.[85] provides a detailed account of recent and ongoing investigations, and the following section describes advances and controversies attending recent studies of catalytic phenomena in water droplets.

F. REACTION ACCELERATION IN/ON WATER DROPLETS

Recent evidence suggests that chemical reactions in micron-sized droplets, films, and emulsions proceed up to a million-fold faster than the same reactions in macroscopic solutions.[87] There appears to be no general explanation for the acceleration mechanism(s), although the droplet interface is thought to play a prominent role, with partial solvation, reagent orientation, extremes of surface acidity or basicity, and large electric fields proposed as reasons for an intrinsic increase in the reaction rate constant within microdroplets.[87] Additional acceleration mechanisms present in many experiments include the rapid evaporation of reagents and/or solvent,[88,89] interfering gas phase [89–91] and wall reactions.[89] The strong influence of the interface in droplets echoes many of the same outstanding questions/uncertainties about the structure and dynamics of macroscale aqueous interfaces raised throughout this Introduction.

A central question is whether the accelerated reaction rates in microdroplets reflect a fundamental change in the rate coefficient for the reaction rather than enriched reactant concentrations - either at the interface or in the bulk - due to evaporation of solvent[92]. Cooks and coworkers,[87] and Ruiz-Lopez et al.[93] argue that the partially solvated environment of the droplet interface can substantially alter the energetics of some reactions relative to those occurring in a

homogenous aqueous solution. There is often a substantial barrier for a reaction in solution that arises from the energy required (~2-20 kcal/mol)[87] to displace the solvation shells around reactants. This is not the case for many analogous gas phase reactions, and explains why, for example, gas phase ion-neutral reactions can proceed ~10^6 faster than in solution. The solvation properties of liquid interfaces are somewhere between those of bulk and gas phases. Narendra *et al.*[94] explored the consequence of partially solvated reagent molecules and transition states at an interface; they observed an increase in energy for specific surface orientations, computed to be as high as 1.6 eV. This increased energy originated from configurations that had lower degrees of solvation around the charged site of a reactant molecule. From these calculations, Narendra *et al.*[94] estimated an upper bound for a rate constant enhancement in microdroplets of 10^4.

A number of studies indicate that microdroplets exhibit unusual acid/base catalysis with droplets sustaining stable long-range ion and pH gradients[95–99] and with some evidence for superacid and basic interfaces.[100] In contrast, other studies[101] observe a homogeneous pH within the droplets, with some evidence that pH is a function of droplet size and is either lower[102–104] or higher[96] or the same[101,105] as the corresponding bulk solution. The acidity or basicity of the air/water interface and whether the interface of charged droplets is somehow different than a flat interface remains a matter of some debate.[44,45,49,50,91,106–108]

It has been proposed that the electric field at the interface of microdroplets plays a central role in accelerating reactions. This is particularly true for those highly charged droplets produced in Electrospray Ionization Mass Spectrometry (ESI-MS) or one of its variants. There are a number of experimental[109] and theoretical studies[110–115] of the field strength at the air/water interface or within droplets with a range of values reported, which are generally on the order of 10 MV/cm and above. As discussed recently by Hao et al.,[116] theoretical determinations of this quantity can be quite challenging. Nevertheless, strong electric fields can alter reaction kinetics by lowering activation energies or redox potentials, by repelling or attracting solutes, and/or altering solvation electrostatics.[110] Strong electric fields also stabilize charge separation in a transition state and activate bonds for dissociation.[117] As shown theoretically by Chamberlayne and Zare[98] and Malevanets and Consta[99], microdroplets can exhibit a substantially altered ion distribution relative to flat surfaces, with droplets exhibiting radial ion concentration gradients, analogous to the pH gradients discussed above. As proposed by Chamberlayne and Zare,[97] these ion gradients may store potential energy that could be used to drive chemical reactions in a way analogous to more familiar electrochemical systems.

It has been suggested that the electric fields in microdroplets also give rise to exotic species that contribute to much of the chemistry now observed in ESI-MS studies of accelerated chemistry. It is interesting to consider how the chemistry observed in the electrokinetic studies of liquid jets, described above, might relate to droplets produced in ESI-MS studies of microdroplet chemistry. Zare and coworkers[118–120] proposed that hydroxyl radicals and a hydrated electron could be produced from interfacial OH^- in the presence of strong electric fields in order to explain the spontaneous formation of H_2O_2 observed in sprayed microdroplets. There are a numbers of studies that have questioned the viability of this H_2O_2 formation mechanism, as well as some quantitative aspects of the experimental observations.[121–124] Additional evidence for spontaneous $OH\cdot$ formation in neutral aqueous aerosols[125] was recently reported and attributed to the mechanism proposed by Zare and coworkers, although counter-intuitively, that study reported a decrease in hydroxyl radical production with increasing pH. Recent theoretical work by Head-Gordon and coworkers[126] reported a decrease in the vertical ionization energy of hydroxide at the air-water interface due to partial solvation. These authors conclude, based upon

their previous work on electric fields[111], that there is a, ". . .small but still significant probability to spontaneously create H_2O_2. . ." via the mechanism originally proposed by Zare and coworkers. Alternatively, Ben-Amotz,[127] Cooks and coworkers,[128–130] have proposed that water radical cations and anions could be formed in bulk water and at the surface of charged droplets, which would explain the rather unusual simultaneous oxidation and reduction of species produced in droplets formed in nanospray mass spectrometry. To support these results, a double layer model of the droplet interface is invoked wherein the strong electric field forms and spatially separates the radical cation and anion pairs into distinct surface layers.

Evaporation of solvent from microdroplets concentrates reactants and naturally accelerates kinetics. In an open macroscale container, it takes a relatively long time to evaporate enough solvent to increase reagent concentrations to accelerate bulk kinetics, and thus in most cases can be neglected or simply eliminated by sealing the container to achieve equilibrium conditions. This is not true of microdroplets experiments that utilize electrospray ionization sources wherein equilibration of the solvent with the surrounding vapor is never achieved. These sources also produce a distribution of droplets sizes and therefore of evaporation rates and droplet lifetimes[131]. The implicit assumption in many of these studies is that the droplet lifetimes are long compared to the microdroplet reaction. Furthermore, it is often assumed that the process by which the droplet is destroyed and its contents converted to detectable ions, during its transit to and into the inlet of the mass spectrometer, does not appreciably affect the observed chemistry.

For example, Lee et al.,[132] reported that the aqueous phase reaction of 2,6-dichlorophenolinedopenol (DCIP) and ascorbic acid is accelerated by 10^3 in colliding microdroplets (*i.e.* measured via droplet fusion mass spectrometry). Based upon the size of the droplet imaged during the reaction (*e.g.* 13 microns), the authors of that study argued that droplet evaporation did not play a significant role in the acceleration mechanism. However, as pointed out by Rovelli *et al.*,[89] the relative velocity of the colliding streams in the experiment likely favors droplet fission rather than fusion, and in all likelihood, there is a large population of smaller droplets not visible to the imaging techniques. Jacobs *et al.*,[90] confirmed that the in-droplet DCIP + ascorbic acid reaction does not have interference from gas phase reactions (discussed below). Chen and Williams[88] recently examined this reaction using fast mixing nanospray theta capillaries that produced 684 nm and 1.84 μm droplets. Using an internal standard for droplet lifetime, they were able to quantitatively measure reaction timescales to determine a range of acceleration factors (10^2-10^7) that scaled with the initial DCIP concentrations of 10^{-2} to 10^2 μM, respectively. They observed no appreciable size dependence with the largest acceleration (10^7) measured for the most dilute initial concentrations (10^{-2} μM). They quantitatively explained their large acceleration factors solely by analyte enrichment inside the droplet due to solvent evaporation.

Finally, in addition to evaporation effects, the presence of gas phase reactions from reagents emanating from the microdroplet themselves can lead to apparent acceleration factors. Zare and coworkers published a series of papers[133,134] wherein they observed the rapid reaction of simple sugars with phosphoric acid in aqueous droplets. They also observed that the products of these reactions (*i.e.*, sugar phosphates) could then further react with nucleobases to form ribonucleosides. Together, these in-droplet reactions are potentially important routes for prebiotic chemistry,[135] since in macroscale aqueous solutions these reactions are thermodynamically unfavorable and kinetically slow. Jacobs *et al.*[90] and Rovelli *et al.*[89] showed through a series of measurements that the sugar phosphate and ribonucleoside products could be

formed in experiments wherein the reagents never resided inside the same microdroplet, thus showing that there is a significant gas phase contribution to the observed chemistry (likely ion-molecule reactions). It is well-known that reactions of ions and neutral molecules are orders of magnitude faster in the gas phase than the liquid phase, hence the potential for gas phase interferences for these types of reactions in ESI generated microdroplets is high, and suitable experimental checks are required prior to any discussion about in droplet acceleration mechanisms. Unfortunately, the vast majority of studies now reporting accelerated chemistry in microdroplets using ESI type approaches do not report such experimental checks for gas phase interferences.

3. ICE INTERFACES

Ice is endemic in our environment and constitutes an entirely different aqueous interface than that of the liquid. Or does it? The ice-vapor interface starts to be disordered – with reportedly liquid-like properties – above 200 K, much lower than the melting point of bulk ice. This disordered layer is often called the "quasi-liquid layer". This quasi-liquid layer plays a critical role in the lubrication of ice surface, gas uptake by ice, and growth of aerosols affecting climate change. Furthermore, ice nucleation process such as heterogeneous ice nucleation, which is bound to the material interface, affects the biological functions of animals in the cold sea as well as technology aiming at controlling friction of ice.

SFG and X-ray spectroscopy have been employed extensively to probe ice interfaces, but until recently, it has been difficult to reliably interpret these measurements. Tang et al.[136] have presented a detailed review of results obtained from theoretical modeling compared with experimental data to reveal the molecular-level structure of ice/air interfaces. Perhaps the most salient aspect of this interface is the long-recognized quasi-liquid (premelting) layer, shown in Figure 6 right panel. Simulations have estimated this layer to be ca. 3 nm at 272 K, scaling logarithmically with temperature to a finite thickness of 6 nm before crossing the melting threshold.[137] Vibrational SFG measurements suggest a bilayer-by-bilayer mechanism as the quasi-liquid-layer grows in thickness, and reports stronger hydrogen bonds for water in the premelting layer than in bulk water.[138,139] Moritz et al.[140] thoroughly characterize these phenomena in their recent detailed study. The opposite of the melting transition of ice is the freezing of ice from the liquid, which has also been studied in much detail. The following paper by Lupi et al.[141] details the complexity resulting from layering disorder, due to random layering of hexagonal and cubic ice layers, which requires major revision of results from classical nucleation theory.

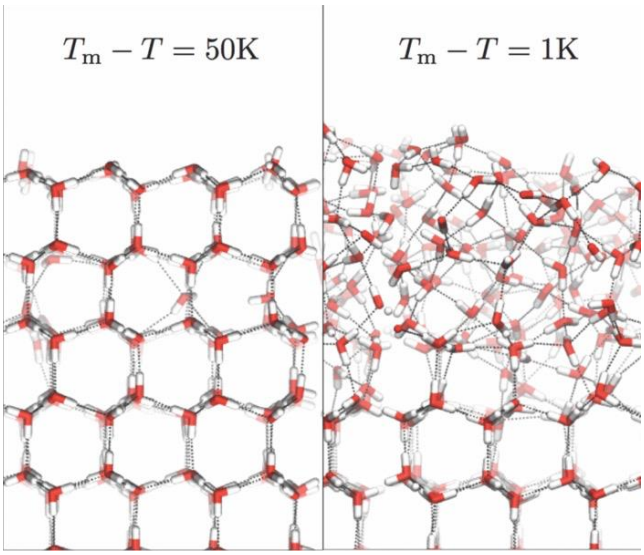

Fig 6: Snapshots of the basal surface of ice I_h far from (left) and close to (right) the melting transition. Reproduced from reference 137, with permission from the American Institute of Physics, copyright 2014.

The investigation and debate regarding the proposed liquid-liquid phase transition in water was continued in 2022. Niinomi et al[142] previously discovered by *in situ* optical microscopy that macroscopic droplets and layers of "high-density unknown water" (HDUW) separated from bulk water by a clear interface, appear at the interface between water and high-density ices (ices III and VI) grown or melted by depressurization or pressurization in a sapphire anvil cell. Very recently, they found that macroscopic droplets and layers of "low-density unknown water" (LDUW) separated from bulk appear at the interface between water and low-density ice (ice I_h) grown or melted by depressurization or pressurization in an electrically regulated sapphire anvil cell. They also determined the ratio between the interfacial tension and the viscosity (the "characteristic velocity"). Their results confirmed that LDUW and HDUW differ from previously observed forms of water, including the quasi-liquid layer observed at air/ice interfaces.

4. SOFT MATTER-WATER INTERFACES

Soft matter ranges from the biological membrane interface to the polymer interface. Biological interfaces often are unstable without water; water drives the self-assembly of biological structures, and through the interaction with interfacial water, their biological function emerges. Polymer interfaces allow control over the hydrophobicity/hydrophilicity, and the variation of the interfacial water properties e.g. pH and temperature, alters the formation of polymers, making polymer materials useful for drug delivery and coating. A particularly interesting soft matter-water interface is the interface that originates from liquid-liquid phase separation in aqueous solutions of polymers and intrinsically disordered proteins. All these interfaces have in common that molecular-level insights into the interactions of these interfaces with interfacial water remain unclear.

In oceanic environments, the surfaces of polymeric micro- or nano-plastics act as a sink for molecular pollutants. Understanding the behavior of molecules at these interfaces is

important to current research, such as water purification. In 2019, the Saykally group used angle-resolved second harmonic scattering (AR-SHS) to predict the mechanism of adsorption of various micropollutants to colloidal polystyrene beads, determining the free energy of adsorption of each species. A displacement methodology was used to study molecules such as caffeine and ascorbic acid, which do not have accessible transitions for resonant AR-SHS studies. For charged molecules, electrostatic interactions contributed to the adsorption behavior, but for molecules with large hydrocarbon regions (even those containing charge), the adsorption was dominated by van der Waals interactions.[143]

Recent work in the group has expanded on the AR-SHS methods to examine other soft-matter surfaces, including silica nanoparticles and metal organic frameworks (MOFs). MOFs such as ZIF-8 are gaining attention in a multitude of fields for their tunability and large surface area. For example, ZIF-8 has been used in part as a colorimetric sensor for CO_2 detection.[144] However, the adsorption dynamics between the colorimetric dye and other precursors with the surface of ZIF-8 are not well-understood. Preliminary work has probed the cationic dye malachite green in a methanolic solution with ZIF-8. Current work reveals a steep increase in SH signal at 200 uM malachite green with 0.1 mg/mL ZIF-8 when samples are probed immediately after preparation. The resulting concentration curve is non-Langmuirian. However, if samples are left to sit overnight, the curve becomes more Langmuirian after an initial dip in signal at 100 uM. So far, these results have been attributed to possible agglomeration of ZIF-8, porous effects, or complex adsorption kinetics. Future work will involve utilizing polarization-resolved SHS to better characterize porous surfaces.

ACKNOWLEDGEMENTS
This work was supported by the Department of Energy, Office of Basic Energy Sciences, through the Chemical Sciences Division at the Lawrence Berkeley National Laboratory, the King Abdullah University of Science and Technology, CALSOLV/RESOLV-Bochum (E.R.), and the UC Office of the President within the Multicampus Research Programs and Initiatives

References

(1) Ahmed, M.; Blum, M.; Crumlin, E. J.; Geissler, P. L.; Head-Gordon, T.; Limmer, D. T.; Mandadapu, K. K.; Saykally, R. J.; Wilson, K. R. Molecular Properties and Chemical Transformations Near Interfaces. *J. Phys. Chem. B* **2021**, *125* (32), 9037–9051. https://doi.org/10.1021/acs.jpcb.1c03756.

(2) Shimizu, T. K.; Maier, S.; Verdaguer, A.; Velasco-Velez, J.-J.; Salmeron, M. Water at Surfaces and Interfaces: From Molecules to Ice and Bulk Liquid. *Prog. Surf. Sci.* **2018**, *93* (4), 87–107. https://doi.org/10.1016/j.progsurf.2018.09.004.

(3) Björneholm, O.; Hansen, M. H.; Hodgson, A.; Liu, L.-M.; Limmer, D. T.; Michaelides, A.; Pedevilla, P.; Rossmeisl, J.; Shen, H.; Tocci, G.; Tyrode, E.; Walz, M.-M.; Werner, J.; Bluhm, H. Water at Interfaces. *Chem. Rev.* **2016**, *116* (13), 7698–7726. https://doi.org/10.1021/acs.chemrev.6b00045.

(4) Geissler, P. L. Water Interfaces, Solvation, and Spectroscopy. *Annu. Rev. Phys. Chem.* **2013**, *64* (1), 317–337. https://doi.org/10.1146/annurev-physchem-040412-110153.

(5) Nagata, Y.; Backus, E. H. G.; Bonn, M. Dynamics of Water Molecules at the Water/Air Interface. In *Encyclopedia of Interfacial Chemistry*; Elsevier, 2018; pp 348–355. https://doi.org/10.1016/B978-0-12-409547-2.13229-9.

(6) Shen, Y. R. *Fundamentals of Sum-Frequency Spectroscopy*, 1st ed.; Cambridge University Press, 2016. https://doi.org/10.1017/CBO9781316162613.

(7) Yu, C.-C.; Seki, T.; Chiang, K.-Y.; Tang, F.; Sun, S.; Bonn, M.; Nagata, Y. Polarization-Dependent Heterodyne-Detected Sum-Frequency Generation Spectroscopy as a Tool to Explore Surface Molecular Orientation and Ångström-Scale Depth Profiling. *J. Phys. Chem. B* **2022**, *126* (33), 6113–6124. https://doi.org/10.1021/acs.jpcb.2c02178.

(8) Petersen, P. B.; Saykally, R. J. ON THE NATURE OF IONS AT THE LIQUID WATER SURFACE. *Annu. Rev. Phys. Chem.* **2006**, *57* (1), 333–364. https://doi.org/10.1146/annurev.physchem.57.032905.104609.

(9) Mizuno, H.; Rizzuto, A. M.; Saykally, R. J. Charge-Transfer-to-Solvent Spectrum of Thiocyanate at the Air/Water Interface Measured by Broadband Deep Ultraviolet Electronic Sum Frequency Generation Spectroscopy. *J. Phys. Chem. Lett.* **2018**, *9* (16), 4753–4757. https://doi.org/10.1021/acs.jpclett.8b01966.

(10) Lam, R. K.; Raj, S. L.; Pascal, T. A.; Pemmaraju, C. D.; Foglia, L.; Simoncig, A.; Fabris, N.; Miotti, P.; Hull, C. J.; Rizzuto, A. M.; Smith, J. W.; Mincigrucci, R.; Masciovecchio, C.; Gessini, A.; Allaria, E.; De Ninno, G.; Diviacco, B.; Roussel, E.; Spampinati, S.; Penco, G.; Di Mitri, S.; Trovò, M.; Danailov, M.; Christensen, S. T.; Sokaras, D.; Weng, T.-C.; Coreno, M.; Poletto, L.; Drisdell, W. S.; Prendergast, D.; Giannessi, L.; Principi, E.; Nordlund, D.; Saykally, R. J.; Schwartz, C. P. Soft X-Ray Second Harmonic Generation as an Interfacial Probe. *Phys. Rev. Lett.* **2018**, *120* (2), 023901. https://doi.org/10.1103/PhysRevLett.120.023901.

(11) Schlesinger, I.; Sivan, U. New Information on the Hydrophobic Interaction Revealed by Frequency Modulation AFM. *Langmuir* **2017**, *33* (10), 2485–2496. https://doi.org/10.1021/acs.langmuir.6b03574.

(12) Gassin, P.-M.; Prelot, B.; Grégoire, B.; Martin-Gassin, G. Second-Harmonic Scattering in Layered Double Hydroxide Colloids: A Microscopic View of Adsorption and Intercalation. *Langmuir* **2018**, *34* (40), 12206–12213. https://doi.org/10.1021/acs.langmuir.8b02161.

(13) Chu, B.; Marchioro, A.; Roke, S. Size Dependence of Second-Harmonic Scattering from Nanoparticles: Disentangling Surface and Electrostatic Contributions. *J. Chem. Phys.* **2023**, *158* (9), 094711. https://doi.org/10.1063/5.0135157.
(14) Roesel, D.; Eremchev, M.; Schönfeldová, T.; Lee, S.; Roke, S. Water as a Contrast Agent to Quantify Surface Chemistry and Physics Using Second Harmonic Scattering and Imaging: A Perspective. *Appl. Phys. Lett.* **2022**, *120* (16), 160501. https://doi.org/10.1063/5.0085807.
(15) Marchioro, A.; Bischoff, M.; Lütgebaucks, C.; Biriukov, D.; Předota, M.; Roke, S. Surface Characterization of Colloidal Silica Nanoparticles by Second Harmonic Scattering: Quantifying the Surface Potential and Interfacial Water Order. *J. Phys. Chem. C* **2019**, *123* (33), 20393–20404. https://doi.org/10.1021/acs.jpcc.9b05482.
(16) Gomopoulos, N.; Lütgebaucks, C.; Sun, Q.; Macias-Romero, C.; Roke, S. Label-Free Second Harmonic and Hyper Rayleigh Scattering with High Efficiency. *Opt. Express* **2013**, *21* (1), 815. https://doi.org/10.1364/OE.21.000815.
(17) Roke, S.; Roeterdink, W. G.; Wijnhoven, J. E. G. J.; Petukhov, A. V.; Kleyn, A. W.; Bonn, M. Vibrational Sum Frequency Scattering from a Submicron Suspension. *Phys. Rev. Lett.* **2003**, *91* (25), 258302. https://doi.org/10.1103/PhysRevLett.91.258302.
(18) Tran, E.; Richmond, G. L. Interfacial Steric and Molecular Bonding Effects Contributing to the Stability of Neutrally Charged Nanoemulsions. *Langmuir* **2021**, *37* (43), 12643–12653. https://doi.org/10.1021/acs.langmuir.1c02020.
(19) Tran, E.; Mapile, A. N.; Richmond, G. L. Peeling Back the Layers: Investigating the Effects of Polyelectrolyte Layering on Surface Structure and Stability of Oil-in-Water Nanoemulsions. *J. Colloid Interface Sci.* **2021**, *599*, 706–716. https://doi.org/10.1016/j.jcis.2021.04.115.
(20) Pullanchery, S.; Kulik, S.; Roke, S. Water Structure at the Hydrophobic Nanodroplet Surface Revealed by Vibrational Sum Frequency Scattering Using Isotopic Dilution. *J. Phys. Chem. B* **2022**, *126* (16), 3186–3192. https://doi.org/10.1021/acs.jpcb.2c01987.
(21) Marchioro, A.; Golbek, T. W.; Chatterley, A. S.; Weidner, T.; Roke, S. A Discrepancy of 107 in Experimental and Theoretical Density Detection Limits of Aerosol Particles by Surface Nonlinear Light Scattering. *Commun. Chem.* **2023**, *6* (1), 114. https://doi.org/10.1038/s42004-023-00903-8.
(22) Willard, A. P.; Chandler, D. Instantaneous Liquid Interfaces. *J. Phys. Chem. B* **2010**, *114* (5), 1954–1958. https://doi.org/10.1021/jp909219k.
(23) Kessler, J.; Elgabarty, H.; Spura, T.; Karhan, K.; Partovi-Azar, P.; Hassanali, A. A.; Kühne, T. D. Structure and Dynamics of the Instantaneous Water/Vapor Interface Revisited by Path-Integral and Ab Initio Molecular Dynamics Simulations. *J. Phys. Chem. B* **2015**, *119* (31), 10079–10086. https://doi.org/10.1021/acs.jpcb.5b04185.
(24) Odendahl, N. L.; Geissler, P. L. Local Ice-like Structure at the Liquid Water Surface. *J. Am. Chem. Soc.* **2022**, *144* (25), 11178–11188. https://doi.org/10.1021/jacs.2c01827.
(25) Bonn, M.; Nagata, Y.; Backus, E. H. G. Molecular Structure and Dynamics of Water at the Water-Air Interface Studied with Surface-Specific Vibrational Spectroscopy. *Angew. Chem. Int. Ed.* **2015**, *54* (19), 5560–5576. https://doi.org/10.1002/anie.201411188.
(26) Cappa, C. D. Isotopic Fractionation of Water during Evaporation. *J. Geophys. Res.* **2003**, *108* (D16), 4525. https://doi.org/10.1029/2003JD003597.
(27) Wilson, K. R.; Schaller, R. D.; Co, D. T.; Saykally, R. J.; Rude, B. S.; Catalano, T.; Bozek, J. D. Surface Relaxation in Liquid Water and Methanol Studied by X-Ray Absorption

Spectroscopy. *J. Chem. Phys.* **2002**, *117* (16), 7738–7744. https://doi.org/10.1063/1.1508364.
(28) Tong, Y.; Kampfrath, T.; Campen, R. K. Experimentally Probing the Libration of Interfacial Water: The Rotational Potential of Water Is Stiffer at the Air/Water Interface than in Bulk Liquid. *Phys. Chem. Chem. Phys.* **2016**, *18* (27), 18424–18430. https://doi.org/10.1039/C6CP01004K.
(29) Cole, W. T. S.; Saykally, R. J. Hydrogen Bond Network Rearrangement Dynamics in Water Clusters: Effects of Intermolecular Vibrational Excitation on Tunneling Rates. *J. Chem. Phys.* **2017**, *147* (6), 064301. https://doi.org/10.1063/1.4997046.
(30) Cole, W. T. S.; Yönder, Ö.; Sheikh, A. A.; Fellers, R. S.; Viant, M. R.; Saykally, R. J.; Farrell, J. D.; Wales, D. J. Terahertz VRT Spectroscopy of the Water Hexamer-H12 Cage: Dramatic Libration-Induced Enhancement of Hydrogen Bond Tunneling Dynamics. *J. Phys. Chem. A* **2018**, *122* (37), 7421–7426. https://doi.org/10.1021/acs.jpca.8b05777.
(31) Rizzuto, A. M.; Cheng, E. S.; Lam, R. K.; Saykally, R. J. Surprising Effects of Hydrochloric Acid on the Water Evaporation Coefficient Observed by Raman Thermometry. *J. Phys. Chem. C* **2017**, *121* (8), 4420–4425. https://doi.org/10.1021/acs.jpcc.6b12851.
(32) Marek, R.; Straub, J. Analysis of the Evaporation Coefficient and the Condensation Coefficient of Water. *Int. J. Heat Mass Transf.* **2001**, *44* (1), 39–53. https://doi.org/10.1016/S0017-9310(00)00086-7.
(33) Smith, J. D.; Cappa, C. D.; Drisdell, W. S.; Cohen, R. C.; Saykally, R. J. Raman Thermometry Measurements of Free Evaporation from Liquid Water Droplets. *J. Am. Chem. Soc.* **2006**, *128* (39), 12892–12898. https://doi.org/10.1021/ja063579v.
(34) Drisdell, W. S.; Cappa, C. D.; Smith, J. D.; Saykally, R. J.; Cohen, R. C. *Determination of the Evaporation Coefficient of D₂O*; preprint; 2008. https://doi.org/10.5194/acpd-8-8565-2008.
(35) Drisdell, W. S.; Saykally, R. J.; Cohen, R. C. Effect of Surface Active Ions on the Rate of Water Evaporation. *J. Phys. Chem. C* **2010**, *114* (27), 11880–11885. https://doi.org/10.1021/jp101726x.
(36) Drisdell, W. S.; Saykally, R. J.; Cohen, R. C. On the Evaporation of Ammonium Sulfate Solution. *Proc. Natl. Acad. Sci.* **2009**, *106* (45), 18897–18901. https://doi.org/10.1073/pnas.0907988106.
(37) Duffey, K. C.; Shih, O.; Wong, N. L.; Drisdell, W. S.; Saykally, R. J.; Cohen, R. C. Evaporation Kinetics of Aqueous Acetic Acid Droplets: Effects of Soluble Organic Aerosol Components on the Mechanism of Water Evaporation. *Phys. Chem. Chem. Phys.* **2013**, *15* (28), 11634. https://doi.org/10.1039/c3cp51148k.
(38) Varilly, P.; Chandler, D. Water Evaporation: A Transition Path Sampling Study. *J. Phys. Chem. B* **2013**, *117* (5), 1419–1428. https://doi.org/10.1021/jp310070y.
(39) Nagata, Y.; Usui, K.; Bonn, M. Molecular Mechanism of Water Evaporation. *Phys. Rev. Lett.* **2015**, *115* (23), 236102. https://doi.org/10.1103/PhysRevLett.115.236102.
(40) Kazemi, M. A.; Zandavi, S. H.; Zargartalebi, M.; Sinton, D.; Elliott, J. A. W. Analysis of the Evaporation Coefficients of Water, Heavy Water, and Methanol in a High Vacuum Environment. *Int. J. Heat Mass Transf.* **2023**, *204*, 123833. https://doi.org/10.1016/j.ijheatmasstransfer.2022.123833.
(41) Gonella, G.; Backus, E. H. G.; Nagata, Y.; Bonthuis, D. J.; Loche, P.; Schlaich, A.; Netz, R. R.; Kühnle, A.; McCrum, I. T.; Koper, M. T. M.; Wolf, M.; Winter, B.; Meijer, G.;

Campen, R. K.; Bonn, M. Water at Charged Interfaces. *Nat. Rev. Chem.* **2021**, *5* (7), 466–485. https://doi.org/10.1038/s41570-021-00293-2.
(42) Petersen, P. B.; Saykally, R. J. Is the Liquid Water Surface Basic or Acidic? Macroscopic vs. Molecular-Scale Investigations. *Chem. Phys. Lett.* **2008**, *458* (4–6), 255–261. https://doi.org/10.1016/j.cplett.2008.04.010.
(43) Petersen, P. B.; Saykally, R. J. Evidence for an Enhanced Hydronium Concentration at the Liquid Water Surface. *J. Phys. Chem. B* **2005**, *109* (16), 7976–7980. https://doi.org/10.1021/jp044479j.
(44) Saykally, R. J. Two Sides of the Acid–Base Story. *Nat. Chem.* **2013**, *5* (2), 82–84. https://doi.org/10.1038/nchem.1556.
(45) Buch, V.; Milet, A.; Vácha, R.; Jungwirth, P.; Devlin, J. P. Water Surface Is Acidic. *Proc. Natl. Acad. Sci.* **2007**, *104* (18), 7342–7347. https://doi.org/10.1073/pnas.0611285104.
(46) Das, S.; Imoto, S.; Sun, S.; Nagata, Y.; Backus, E. H. G.; Bonn, M. Nature of Excess Hydrated Proton at the Water–Air Interface. *J. Am. Chem. Soc.* **2020**, *142* (2), 945–952. https://doi.org/10.1021/jacs.9b10807.
(47) Tian, C.; Ji, N.; Waychunas, G. A.; Shen, Y. R. Interfacial Structures of Acidic and Basic Aqueous Solutions. *J. Am. Chem. Soc.* **2008**, *130* (39), 13033–13039. https://doi.org/10.1021/ja8021297.
(48) Beattie, J. K.; Djerdjev, A. M.; Warr, G. G. The Surface of Neat Water Is Basic. *Faraday Discuss* **2009**, *141*, 31–39. https://doi.org/10.1039/B805266B.
(49) Tse, Y.-L. S.; Chen, C.; Lindberg, G. E.; Kumar, R.; Voth, G. A. Propensity of Hydrated Excess Protons and Hydroxide Anions for the Air–Water Interface. *J. Am. Chem. Soc.* **2015**, *137* (39), 12610–12616. https://doi.org/10.1021/jacs.5b07232.
(50) Mundy, C. J.; Kuo, I.-F. W.; Tuckerman, M. E.; Lee, H.-S.; Tobias, D. J. Hydroxide Anion at the Air–Water Interface. *Chem. Phys. Lett.* **2009**, *481* (1–3), 2–8. https://doi.org/10.1016/j.cplett.2009.09.003.
(51) Giberti, F.; Hassanali, A. A. The Excess Proton at the Air-Water Interface: The Role of Instantaneous Liquid Interfaces. *J. Chem. Phys.* **2017**, *146* (24), 244703. https://doi.org/10.1063/1.4986082.
(52) Zhang, P.; Feng, M.; Xu, X. *Double-Layer Distribution of Hydronium and Hydroxide Ions in the Air-Water Interface*; preprint; Chemistry, 2023. https://doi.org/10.26434/chemrxiv-2023-5l2wf.
(53) Jungwirth, P.; Tobias, D. J. Ions at the Air/Water Interface. *J. Phys. Chem. B* **2002**, *106* (25), 6361–6373. https://doi.org/10.1021/jp020242g.
(54) Raymond, E. A.; Richmond, G. L. Probing the Molecular Structure and Bonding of the Surface of Aqueous Salt Solutions. *J. Phys. Chem. B* **2004**, *108* (16), 5051–5059. https://doi.org/10.1021/jp037725k.
(55) Petersen, P. B.; Saykally, R. J. Confirmation of Enhanced Anion Concentration at the Liquid Water Surface. *Chem. Phys. Lett.* **2004**, *397* (1–3), 51–55. https://doi.org/10.1016/j.cplett.2004.08.049.
(56) Otten, D. E.; Shaffer, P. R.; Geissler, P. L.; Saykally, R. J. Elucidating the Mechanism of Selective Ion Adsorption to the Liquid Water Surface. *Proc. Natl. Acad. Sci.* **2012**, *109* (3), 701–705. https://doi.org/10.1073/pnas.1116169109.
(57) Wang, Y.; Sinha, S.; Desai, P. R.; Jing, H.; Das, S. Ion at Air–Water Interface Enhances Capillary Wave Fluctuations: Energetics of Ion Adsorption. *J. Am. Chem. Soc.* **2018**, *140* (40), 12853–12861. https://doi.org/10.1021/jacs.8b06205.

(58) McCaffrey, D. L.; Nguyen, S. C.; Cox, S. J.; Weller, H.; Alivisatos, A. P.; Geissler, P. L.; Saykally, R. J. Mechanism of Ion Adsorption to Aqueous Interfaces: Graphene/Water vs. Air/Water. *Proc. Natl. Acad. Sci.* **2017**, *114* (51), 13369–13373. https://doi.org/10.1073/pnas.1702760114.
(59) Devlin, S. W.; McCaffrey, D. L.; Saykally, R. J. Characterizing Anion Adsorption to Aqueous Interfaces: Toluene–Water versus Air–Water. *J. Phys. Chem. Lett.* **2022**, *13* (1), 222–228. https://doi.org/10.1021/acs.jpclett.1c03816.
(60) Devlin, S. W.; Benjamin, I.; Saykally, R. J. On the Mechanisms of Ion Adsorption to Aqueous Interfaces: Air-Water vs. Oil-Water. *Proc. Natl. Acad. Sci.* **2022**, *119* (42), e2210857119. https://doi.org/10.1073/pnas.2210857119.
(61) Onorato, R. M.; Otten, D. E.; Saykally, R. J. Measurement of Bromide Ion Affinities for the Air/Water and Dodecanol/Water Interfaces at Molar Concentrations by UV Second Harmonic Generation Spectroscopy. *J. Phys. Chem. C* **2010**, *114* (32), 13746–13751. https://doi.org/10.1021/jp103454r.
(62) Bhattacharyya, D.; Mizuno, H.; Rizzuto, A. M.; Zhang, Y.; Saykally, R. J.; Bradforth, S. E. New Insights into the Charge-Transfer-to-Solvent Spectrum of Aqueous Iodide: Surface versus Bulk. *J. Phys. Chem. Lett.* **2020**, *11* (5), 1656–1661. https://doi.org/10.1021/acs.jpclett.9b03857.
(63) Limmer, D. T.; Willard, A. P.; Madden, P.; Chandler, D. Hydration of Metal Surfaces Can Be Dynamically Heterogeneous and Hydrophobic. *Proc. Natl. Acad. Sci.* **2013**, *110* (11), 4200–4205. https://doi.org/10.1073/pnas.1301596110.
(64) Limmer, D. T.; Willard, A. P.; Madden, P. A.; Chandler, D. Water Exchange at a Hydrated Platinum Electrode Is Rare and Collective. *J. Phys. Chem. C* **2015**, *119* (42), 24016–24024. https://doi.org/10.1021/acs.jpcc.5b08137.
(65) Willard, A. P.; Limmer, D. T.; Madden, P. A.; Chandler, D. Characterizing Heterogeneous Dynamics at Hydrated Electrode Surfaces. *J. Chem. Phys.* **2013**, *138* (18), 184702. https://doi.org/10.1063/1.4803503.
(66) Bellarosa, L.; García-Muelas, R.; Revilla-López, G.; López, N. Diversity at the Water–Metal Interface: Metal, Water Thickness, and Confinement Effects. *ACS Cent. Sci.* **2016**, *2* (2), 109–116. https://doi.org/10.1021/acscentsci.5b00349.
(67) Groß, A.; Sakong, S. Ab Initio Simulations of Water/Metal Interfaces. *Chem. Rev.* **2022**, *122* (12), 10746–10776. https://doi.org/10.1021/acs.chemrev.1c00679.
(68) Sundararaman, R.; Vigil-Fowler, D.; Schwarz, K. Improving the Accuracy of Atomistic Simulations of the Electrochemical Interface. *Chem. Rev.* **2022**, *122* (12), 10651–10674. https://doi.org/10.1021/acs.chemrev.1c00800.
(69) Piontek, S. M.; Naujoks, D.; Tabassum, T.; DelloStritto, M. J.; Jaugstetter, M.; Hosseini, P.; Corva, M.; Ludwig, A.; Tschulik, K.; Klein, M. L.; Petersen, P. B. Probing the Gold/Water Interface with Surface-Specific Spectroscopy. *ACS Phys. Chem. Au* **2023**, *3* (1), 119–129. https://doi.org/10.1021/acsphyschemau.2c00044.
(70) Wallentine, S.; Bandaranayake, S.; Biswas, S.; Baker, L. R. Plasmon-Resonant Vibrational Sum Frequency Generation of Electrochemical Interfaces: Direct Observation of Carbon Dioxide Electroreduction on Gold. *J. Phys. Chem. A* **2020**, *124* (39), 8057–8064. https://doi.org/10.1021/acs.jpca.0c04268.
(71) Ge, A.; Videla, P. E.; Lee, G. L.; Rudshteyn, B.; Song, J.; Kubiak, C. P.; Batista, V. S.; Lian, T. Interfacial Structure and Electric Field Probed by *in Situ* Electrochemical

Vibrational Stark Effect Spectroscopy and Computational Modeling. *J. Phys. Chem. C* **2017**, *121* (34), 18674–18682. https://doi.org/10.1021/acs.jpcc.7b05563.
(72) Rey, N. G.; Dlott, D. D. Studies of Electrochemical Interfaces by Broadband Sum Frequency Generation. *J. Electroanal. Chem.* **2017**, *800*, 114–125. https://doi.org/10.1016/j.jelechem.2016.12.023.
(73) Kruusma, J.; Tõnisoo, A.; Pärna, R.; Nõmmiste, E.; Lust, E. In Situ XPS Studies of Electrochemically Positively Polarized Molybdenum Carbide Derived Carbon Double Layer Capacitor Electrode. *J. Electrochem. Soc.* **2014**, *161* (9), A1266–A1277. https://doi.org/10.1149/2.0641409jes.
(74) Aydogan Gokturk, P.; Sujanani, R.; Qian, J.; Wang, Y.; Katz, L. E.; Freeman, B. D.; Crumlin, E. J. The Donnan Potential Revealed. *Nat. Commun.* **2022**, *13* (1), 5880. https://doi.org/10.1038/s41467-022-33592-3.
(75) Shchukarev, A. XPS at Solid–Aqueous Solution Interface. *Adv. Colloid Interface Sci.* **2006**, *122* (1–3), 149–157. https://doi.org/10.1016/j.cis.2006.06.015.
(76) Lichterman, M. F.; Richter, M. H.; Brunschwig, B. S.; Lewis, N. S.; Lewerenz, H.-J. Operando X-Ray Photoelectron Spectroscopic Investigations of the Electrochemical Double Layer at Ir/KOH(Aq) Interfaces. *J. Electron Spectrosc. Relat. Phenom.* **2017**, *221*, 99–105. https://doi.org/10.1016/j.elspec.2017.03.011.
(77) Duffin, A. M.; Saykally, R. J. Electrokinetic Hydrogen Generation from Liquid Water Microjets. *J. Phys. Chem. C* **2007**, *111* (32), 12031–12037. https://doi.org/10.1021/jp072994m.
(78) Duffin, A. M.; Saykally, R. J. Electrokinetic Power Generation from Liquid Water Microjets. *J. Phys. Chem. C* **2008**, *112* (43), 17018–17022. https://doi.org/10.1021/jp8015276.
(79) Kelly, D. N.; Lam, R. K.; Duffin, A. M.; Saykally, R. J. Exploring Solid/Aqueous Interfaces with Ultradilute Electrokinetic Analysis of Liquid Microjets. *J. Phys. Chem. C* **2013**, *117* (24), 12702–12706. https://doi.org/10.1021/jp403583r.
(80) Lam, R. K.; Shih, O.; Smith, J. W.; Sheardy, A. T.; Rizzuto, A. M.; Prendergast, D.; Saykally, R. J. Electrokinetic Detection for X-Ray Spectra of Weakly Interacting Liquids: N-Decane and n-Nonane. *J. Chem. Phys.* **2014**, *140* (23), 234202. https://doi.org/10.1063/1.4882901.
(81) Schwierz, N.; Lam, R. K.; Gamlieli, Z.; Tills, J. J.; Leung, A.; Geissler, P. L.; Saykally, R. J. Hydrogen and Electric Power Generation from Liquid Microjets: Design Principles for Optimizing Conversion Efficiency. *J. Phys. Chem. C* **2016**, *120* (27), 14513–14521. https://doi.org/10.1021/acs.jpcc.6b03788.
(82) Xie, Y.; Bos, D.; De Vreede, L. J.; De Boer, H. L.; Van Der Meulen, M.-J.; Versluis, M.; Sprenkels, A. J.; Van Den Berg, A.; Eijkel, J. C. T. High-Efficiency Ballistic Electrostatic Generator Using Microdroplets. *Nat. Commun.* **2014**, *5* (1), 3575. https://doi.org/10.1038/ncomms4575.
(83) Li, C.; Meng, P.; Jiang, H.; Hu, X. Power Generation from Microjet Array of Liquid Water. *J. Phys. Appl. Phys.* **2018**, *51* (28), 285501. https://doi.org/10.1088/1361-6463/aacaa5.
(84) Zhang, J.; Zhan, K.; Wang, S.; Hou, X. Soft Interface Design for Electrokinetic Energy Conversion. *Soft Matter* **2020**, *16* (12), 2915–2927. https://doi.org/10.1039/C9SM02506E.
(85) Ruiz-Lopez, M. F.; Francisco, J. S.; Martins-Costa, M. T. C.; Anglada, J. M. Molecular Reactions at Aqueous Interfaces. *Nat. Rev. Chem.* **2020**, *4* (9), 459–475. https://doi.org/10.1038/s41570-020-0203-2.

(86) Limmer, D. T.; Götz, A. W.; Bertram, T. H.; Nathanson, G. M. Molecular Insights into Chemical Reactions at Aqueous Aerosol Interfaces. **2023**. https://doi.org/10.48550/ARXIV.2306.13811.
(87) Wei, Z.; Li, Y.; Cooks, R. G.; Yan, X. Accelerated Reaction Kinetics in Microdroplets: Overview and Recent Developments. *Annu. Rev. Phys. Chem.* **2020**, *71* (1), 31–51. https://doi.org/10.1146/annurev-physchem-121319-110654.
(88) Chen, C. J.; Williams, E. R. The Role of Analyte Concentration in Accelerated Reaction Rates in Evaporating Droplets. *Chem. Sci.* **2023**, *14* (18), 4704–4713. https://doi.org/10.1039/D3SC00259D.
(89) Rovelli, G.; Jacobs, M. I.; Willis, M. D.; Rapf, R. J.; Prophet, A. M.; Wilson, K. R. A Critical Analysis of Electrospray Techniques for the Determination of Accelerated Rates and Mechanisms of Chemical Reactions in Droplets. *Chem Sci* **2020**, *11* (48), 13026–13043. https://doi.org/10.1039/d0sc04611f.
(90) Jacobs, M. I.; Davis, R. D.; Rapf, R. J.; Wilson, K. R. Studying Chemistry in Micro-Compartments by Separating Droplet Generation from Ionization. *J Am Soc Mass Spectrom* **2019**, *30* (2). https://doi.org/10.1007/s13361-018-2091-y.
(91) Gallo, A.; Farinha, A. S. F.; Dinis, M.; Emwas, A.-H.; Santana, A.; Nielsen, R. J.; Goddard, W. A.; Mishra, H. The Chemical Reactions in Electrosprays of Water Do Not Always Correspond to Those at the Pristine Air–Water Interface. *Chem. Sci.* **2019**, *10* (9), 2566–2577. https://doi.org/10.1039/C8SC05538F.
(92) Kevin R. Wilson; Alexander M. Prophet. Chemical Kinetics in Microdroplets. *Annu. Rev. Phys. Chem* **2023**.
(93) Ruiz-López, M.; Martins-Costa, M. Disentangling Reaction Rate Acceleration in Water Microdroplets. *Phys. Chem. Chem. Phys.* **12AD**, *24*. https://doi.org/10.1039/D2CP04998H.
(94) Narendra, N.; Chen, X.; Wang, J.; Charles, J.; Cooks, R. G.; Kubis, T. Quantum Mechanical Modeling of Reaction Rate Acceleration in Microdroplets. *J. Phys. Chem. A* **2020**, *124* (24), 4984–4989. https://doi.org/10.1021/acs.jpca.0c03225.
(95) Gong, K.; Ao, J.; Li, K.; Liu, L.; Liu, Y.; Xu, G.; Wang, T.; Cheng, H.; Wang, Z.; Zhang, X.; Wei, H.; George, C.; Mellouki, A.; Herrmann, H.; Wang, L.; Chen, J.; Ji, M.; Zhang, L.; Francisco, J. S. Imaging of PH Distribution inside Individual Microdroplet by Stimulated Raman Microscopy. *Proc. Natl. Acad. Sci.* **2023**, *120* (20), e2219588120. https://doi.org/10.1073/pnas.2219588120.
(96) Wei, H.; Vejerano, E. P.; Leng, W.; Huang, Q.; Willner, M. R.; Marr, L. C.; Vikesland, P. J. Aerosol Microdroplets Exhibit a Stable PH Gradient. *Proc. Natl. Acad. Sci.* **2018**, *115* (28), 7272–7277. https://doi.org/10.1073/pnas.1720488115.
(97) Chamberlayne, C. F.; Zare, R. N. Microdroplets Can Act as Electrochemical Cells. *J. Chem. Phys.* **2022**, *156* (5). https://doi.org/10.1063/5.0078281.
(98) Chamberlayne, C. F.; Zare, R. N. Simple Model for the Electric Field and Spatial Distribution of Ions in a Microdroplet. *J. Chem. Phys.* **2020**, *152* (18), 184702. https://doi.org/10.1063/5.0006550.
(99) Malevanets, A.; Consta, S. Variation of Droplet Acidity during Evaporation. *J. Chem. Phys.* **2013**, *138* (18). https://doi.org/10.1063/1.4804303.
(100) Huang, K.-H.; Wei, Z.; Cooks, R. G. Accelerated Reactions of Amines with Carbon Dioxide Driven by Superacid at the Microdroplet Interface. *Chem. Sci.* **2021**, *12* (6), 2242–2250. https://doi.org/10.1039/D0SC05625A.

(101) Li, M.; Kan, Y.; Su, H.; Pöschl, U.; Parekh, S. H.; Bonn, M.; Cheng, Y. Spatial Homogeneity of PH in Aerosol Microdroplets. *Chem* **2023**, *9* (4), 1036–1046. https://doi.org/10.1016/j.chempr.2023.02.019.
(102) Craig, R. L.; Peterson, P. K.; Nandy, L.; Lei, Z.; Hossain, M. A.; Camarena, S.; Dodson, R. A.; Cook, R. D.; Dutcher, C. S.; Ault, A. P. Direct Determination of Aerosol PH: Size-Resolved Measurements of Submicrometer and Supermicrometer Aqueous Particles. *Anal. Chem.* **2018**, *90* (19), 11232–11239. https://doi.org/10.1021/acs.analchem.8b00586.
(103) Rindelaub, J. D.; Craig, R. L.; Nandy, L.; Bondy, A. L.; Dutcher, C. S.; Shepson, P. B.; Ault, A. P. Direct Measurement of PH in Individual Particles via Raman Microspectroscopy and Variation in Acidity with Relative Humidity. *J. Phys. Chem. A* **2016**, *120* (6), 911–917. https://doi.org/10.1021/acs.jpca.5b12699.
(104) Coddens, E. M.; Angle, K. J.; Grassian, V. H. Titration of Aerosol PH through Droplet Coalescence. *J. Phys. Chem. Lett.* **2019**, *10* (15), 4476–4483. https://doi.org/10.1021/acs.jpclett.9b00757.
(105) Brown, E. K.; Rovelli, G.; Wilson, K. R. PH Jump Kinetics in Colliding Microdroplets: Accelerated Synthesis of Azamonardine from Dopamine and Resorcinol. *Chem. Sci.* **2023**, *14* (23), 6430–6442. https://doi.org/10.1039/D3SC01576A.
(106) Colussi, A. J. Can the PH at the Air/Water Interface Be Different from the PH of Bulk Water? *Proc. Natl. Acad. Sci.* **2018**, *115* (34), E7887–E7887. https://doi.org/10.1073/pnas.1811632115.
(107) Mishra, H.; Enami, S.; Nielsen, R. J.; Stewart, L. A.; Hoffmann, M. R.; Goddard, W. A.; Colussi, A. J. Brønsted Basicity of the Air–Water Interface. *Proc. Natl. Acad. Sci.* **2012**, *109* (46), 18679–18683. https://doi.org/10.1073/pnas.1209307109.
(108) Bai, C.; Herzfeld, J. Surface Propensities of the Self-Ions of Water. *ACS Cent. Sci.* **2016**, *2* (4), 225–231. https://doi.org/10.1021/acscentsci.6b00013.
(109) Xiong, H.; Lee, J. K.; Zare, R. N.; Min, W. Strong Electric Field Observed at the Interface of Aqueous Microdroplets. *J. Phys. Chem. Lett.* **2020**, *11* (17), 7423–7428. https://doi.org/10.1021/acs.jpclett.0c02061.
(110) Martins-Costa, M. T. C.; Ruiz-López, M. F. Electrostatics and Chemical Reactivity at the Air–Water Interface. *J. Am. Chem. Soc.* **2023**, *145* (2), 1400–1406. https://doi.org/10.1021/jacs.2c12089.
(111) Hao, H.; Leven, I.; Head-Gordon, T. Can Electric Fields Drive Chemistry for an Aqueous Microdroplet? *Nat. Commun.* **2022**, *13* (1), 280. https://doi.org/10.1038/s41467-021-27941-x.
(112) Kathmann, S. M.; Kuo, I. F. W.; Mundy, C. J.; Schenter, G. K. Understanding the Surface Potential of Water. *J. Phys. Chem. B* **2011**, *115* (15), 4369–4377. https://doi.org/10.1021/jp1116036.
(113) Leung, K. Surface Potential at the Air−Water Interface Computed Using Density Functional Theory. *J. Phys. Chem. Lett.* **2010**, *1* (2), 496–499. https://doi.org/10.1021/jz900268s.
(114) Kwan, V.; Malevanets, A.; Consta, S. Where Do the Ions Reside in a Highly Charged Droplet? *J. Phys. Chem. A* **2019**, *123* (43), 9298–9310. https://doi.org/10.1021/acs.jpca.9b03368.
(115) Kwan, V.; Consta, S. Bridging Electrostatic Properties between Nanoscopic and Microscopic Highly Charged Droplets. *Chem. Phys. Lett.* **2020**, *746*, 137238. https://doi.org/10.1016/j.cplett.2020.137238.

(116) Hao, H.; Ruiz Pestana, L.; Qian, J.; Liu, M.; Xu, Q.; Head-Gordon, T. Chemical Transformations and Transport Phenomena at Interfaces. *WIREs Comput. Mol. Sci.* **2023**, *13* (2), e1639. https://doi.org/10.1002/wcms.1639.
(117) Mondal, S.; Acharya, S.; Biswas, R.; Bagchi, B.; Zare, R. N. Enhancement of Reaction Rate in Small-Sized Droplets: A Combined Analytical and Simulation Study. *J. Chem. Phys.* **2018**, *148* (24). https://doi.org/10.1063/1.5030114.
(118) Lee, J. K.; Walker, K. L.; Han, H. S.; Kang, J.; Prinz, F. B.; Waymouth, R. M.; Nam, H. G.; Zare, R. N. Spontaneous Generation of Hydrogen Peroxide from Aqueous Microdroplets. *Proc. Natl. Acad. Sci.* **2019**, *116* (39), 19294–19298. https://doi.org/10.1073/pnas.1911883116.
(119) Lee, J. K.; Han, H. S.; Chaikasetsin, S.; Marron, D. P.; Waymouth, R. M.; Prinz, F. B.; Zare, R. N. Condensing Water Vapor to Droplets Generates Hydrogen Peroxide. *Proc. Natl. Acad. Sci.* **2020**, *117* (49), 30934–30941. https://doi.org/10.1073/pnas.2020158117.
(120) Mehrgardi, M. A.; Mofidfar, M.; Zare, R. N. Sprayed Water Microdroplets Are Able to Generate Hydrogen Peroxide Spontaneously. *J. Am. Chem. Soc.* **2022**, *144* (17), 7606–7609. https://doi.org/10.1021/jacs.2c02890.
(121) Gallo Jr, A.; Musskopf, N. H.; Liu, X.; Yang, Z.; Petry, J.; Zhang, P.; Thoroddsen, S.; Im, H.; Mishra, H. On the Formation of Hydrogen Peroxide in Water Microdroplets. *Chem. Sci.* **2022**, *13* (9), 2574–2583. https://doi.org/10.1039/D1SC06465G.
(122) Nguyen, D.; Lyu, P.; Nguyen, S. C. Experimental and Thermodynamic Viewpoints on Claims of a Spontaneous H2O2 Formation at the Air–Water Interface. *J. Phys. Chem. B* **2023**, *127* (11), 2323–2330. https://doi.org/10.1021/acs.jpcb.2c07394.
(123) Nguyen, D.; Nguyen, S. C. Revisiting the Effect of the Air–Water Interface of Ultrasonically Atomized Water Microdroplets on H2O2 Formation. *J. Phys. Chem. B* **2022**, *126* (16), 3180–3185. https://doi.org/10.1021/acs.jpcb.2c01310.
(124) Musskopf, N. H.; Gallo, A., Jr.; Zhang, P.; Petry, J.; Mishra, H. The Air–Water Interface of Water Microdroplets Formed by Ultrasonication or Condensation Does Not Produce H2O2. *J. Phys. Chem. Lett.* **2021**, *12* (46), 11422–11429. https://doi.org/10.1021/acs.jpclett.1c02953.
(125) Li, K.; Guo, Y.; Nizkorodov, S. A.; Rudich, Y.; Angelaki, M.; Wang, X.; An, T.; Perrier, S.; George, C. Spontaneous Dark Formation of OH Radicals at the Interface of Aqueous Atmospheric Droplets. *Proc. Natl. Acad. Sci.* **2023**, *120* (15), e2220228120. https://doi.org/10.1073/pnas.2220228120.
(126) Heindel, J. P.; Hao, H.; LaCour, R. A.; Head-Gordon, T. Spontaneous Formation of Hydrogen Peroxide in Water Microdroplets. *J. Phys. Chem. Lett.* **2022**, *13* (43), 10035–10041. https://doi.org/10.1021/acs.jpclett.2c01721.
(127) Ben-Amotz, D. Electric Buzz in a Glass of Pure Water. *Science* **2022**, *376* (6595), 800–801. https://doi.org/10.1126/science.abo3398.
(128) Wang, M.; Gao, X.-F.; Su, R.; He, P.; Cheng, Y.-Y.; Li, K.; Mi, D.; Zhang, X.; Zhang, X.; Chen, H.; Cooks, R. G. Abundant Production of Reactive Water Radical Cations under Ambient Conditions. *CCS Chem.* **2022**, *4* (4), 1224–1231. https://doi.org/10.31635/ccschem.021.202101427.
(129) Qiu, L.; Cooks, R. G. Simultaneous and Spontaneous Oxidation and Reduction in Microdroplets by the Water Radical Cation/Anion Pair. *Angew. Chem. Int. Ed.* **2022**, *61* (41), e202210765. https://doi.org/10.1002/anie.202210765.

(130) Qiu, L.; Morato, N. M.; Huang, K.-H.; Cooks, R. G. Spontaneous Water Radical Cation Oxidation at Double Bonds in Microdroplets. *Front. Chem.* **2022**, *10:903774.* https://doi.org/10.3389/fchem.2022.903774.
(131) Xia, Z.; Williams, E. R. Effect of Droplet Lifetime on Where Ions Are Formed in Electrospray Ionization. *The Analyst* **2019**, *144* (1), 237–248. https://doi.org/10.1039/C8AN01824C.
(132) Lee, J. K.; Kim, S.; Nam, H. G.; Zare, R. N. Microdroplet Fusion Mass Spectrometry for Fast Reaction Kinetics. *Proc. Natl. Acad. Sci.* **2015**, *112* (13), 3898–3903. https://doi.org/10.1073/pnas.1503689112.
(133) Nam, I.; Lee, J. K.; Nam, H. G.; Zare, R. N. Abiotic Production of Sugar Phosphates and Uridine Ribonucleoside in Aqueous Microdroplets. *Proc. Natl. Acad. Sci.* **2017**, *114* (47), 12396–12400. https://doi.org/10.1073/pnas.1714896114.
(134) Nam, I.; Nam, H. G.; Zare, R. N. Abiotic Synthesis of Purine and Pyrimidine Ribonucleosides in Aqueous Microdroplets. *Proc. Natl. Acad. Sci.* **2018**, *115* (1), 36–40. https://doi.org/10.1073/pnas.1718559115.
(135) Vaida, V. Prebiotic Phosphorylation Enabled by Microdroplets. *Proc. Natl. Acad. Sci.* **2017**, *114* (47), 12359–12361. https://doi.org/10.1073/pnas.1717373114.
(136) Tang, F.; Ohto, T.; Sun, S.; Rouxel, J. R.; Imoto, S.; Backus, E. H. G.; Mukamel, S.; Bonn, M.; Nagata, Y. Molecular Structure and Modeling of Water–Air and Ice–Air Interfaces Monitored by Sum-Frequency Generation. *Chem. Rev.* **2020**, *120* (8), 3633–3667. https://doi.org/10.1021/acs.chemrev.9b00512.
(137) Limmer, D. T.; Chandler, D. Premelting, Fluctuations, and Coarse-Graining of Water-Ice Interfaces. *J. Chem. Phys.* **2014**, *141* (18), 18C505. https://doi.org/10.1063/1.4895399.
(138) Sánchez, M. A.; Kling, T.; Ishiyama, T.; Van Zadel, M.-J.; Bisson, P. J.; Mezger, M.; Jochum, M. N.; Cyran, J. D.; Smit, W. J.; Bakker, H. J.; Shultz, M. J.; Morita, A.; Donadio, D.; Nagata, Y.; Bonn, M.; Backus, E. H. G. Experimental and Theoretical Evidence for Bilayer-by-Bilayer Surface Melting of Crystalline Ice. *Proc. Natl. Acad. Sci.* **2017**, *114* (2), 227–232. https://doi.org/10.1073/pnas.1612893114.
(139) Shultz, M. J. Ice Surfaces. *Annu. Rev. Phys. Chem.* **2017**, *68* (1), 285–304. https://doi.org/10.1146/annurev-physchem-052516-044813.
(140) Moritz, C.; Geissler, P. L.; Dellago, C. The Microscopic Mechanism of Bulk Melting of Ice. *J. Chem. Phys.* **2021**, *155* (12), 124501. https://doi.org/10.1063/5.0064380.
(141) Lupi, L.; Hudait, A.; Peters, B.; Grünwald, M.; Gotchy Mullen, R.; Nguyen, A. H.; Molinero, V. Role of Stacking Disorder in Ice Nucleation. *Nature* **2017**, *551* (7679), 218–222. https://doi.org/10.1038/nature24279.
(142) Niinomi, H.; Kouch, A.; Hama, T.; Nada, H.; Yamazaki, T.; Kimura, Y. Low- and High-Density Unknown Waters at Ice–Water Interfaces. *J. Phys. Chem. Lett.* **2022**, *13* (19), 4251–4256. https://doi.org/10.1021/acs.jpclett.2c00660.
(143) Cole, W. T. S.; Wei, H.; Nguyen, S. C.; Harris, C. B.; Miller, D. J.; Saykally, R. J. Dynamics of Micropollutant Adsorption to Polystyrene Surfaces Probed by Angle-Resolved Second Harmonic Scattering. *J. Phys. Chem. C* **2019**, *123* (23), 14362–14369. https://doi.org/10.1021/acs.jpcc.9b01146.
(144) Davey, A. K.; Gao, X.; Xia, Y.; Li, Z.; Dods, M. N.; Delacruz, S.; Pan, A.; Swamy, S.; Gardner, D.; Carraro, C.; Maboudian, R. Amine-Functionalized Metal-Organic Framework ZIF-8 toward Colorimetric CO2 Sensing in Indoor Air Environment. *Sens. Actuators B Chem.* **2021**, *344*, 130313. https://doi.org/10.1016/j.snb.2021.130313.

****
****